Binghamton University
The Open Repository @ Binghamton (The ORB)

Undergraduate Honors Theses | Dissertations, Theses and Capstones

5-11-2022

Characterization of bimetallic silver-copper nanoinks with hydroxyethyl-cellulose additives

Daniel Brunick
Binghamton University--SUNY, dbrunic1@binghamton.edu

Follow this and additional works at: https://orb.binghamton.edu/undergrad_honors_theses

 Part of the Chemistry Commons

Recommended Citation

Brunick, Daniel, "Characterization of bimetallic silver-copper nanoinks with hydroxyethyl-cellulose additives" (2022). *Undergraduate Honors Theses*. 12.
https://orb.binghamton.edu/undergrad_honors_theses/12

This Thesis is brought to you for free and open access by the Dissertations, Theses and Capstones at The Open Repository @ Binghamton (The ORB). It has been accepted for inclusion in Undergraduate Honors Theses by an authorized administrator of The Open Repository @ Binghamton (The ORB). For more information, please contact ORB@binghamton.edu.

CHARACTERIZATION OF BIMETALLIC SILVER-COPPER NANOINKS WITH HYDROXYETHYL-CELLULOSE ADDITIVES

BY
DANIEL BRUNICK
BS, STATE UNIVERSITY OF NEW YORK AT BINGHAMTON, 2022
HONORS THESIS

Submitted in partial fulfillment of the requirements for
Distinguished Independent Work in Chemistry
In the Harpur College of
Binghamton University
State University of New York
2022

© Copyright by Daniel Brunick 2022

All Rights Reserved

Accepted in partial fulfillment of the requirements for Distinguished Independent Work in Chemistry

State University of New York at Binghamton

2022

Dr. Chuan-Jian Zhong

Advisor, Committee member

Department of Chemistry _____ **May 11, 2022**

Dr. Huiyuan Guo

Committee member

Department of Chemistry _____ **May 11, 2022**

Dr. Jennifer Hirschi

Committee member

Department of Chemistry _____ **May 11, 2022**

I dedicate this work to those who opened the opportunity for research to me, whose kindness and support have been a godsend.

ABSTRACT

Coinage metal nanoparticles remain an intriguing subject for research due to their industrial versatility. Primary applications of coinage metal nanoparticles include printed electronics, solar panels, and sensors. Inks formulated with the nanoparticles are conductive and thus useful for fabricating sensors. Silver-copper nanoalloy inks are viable for the fabrication of flexible sensing devices for the detection of volatile organic compounds. One of the challenges is the ability to synthesize composition-controllable alloy nanoparticles at room temperature through wet chemical methods and achieve controllable sintering at room temperature. This work addresses the challenges by investigating the room-temperature synthesis of silver-copper alloy nanoparticles and the ink formulation with additives for controllable room-temperature sintering. Cellulose and other compounds derived from this natural polymer are explored for manipulating the ink viscosity and the electrical resistance. Results from the measurements of the electrical resistances of printed devices with the silver-copper nanoalloy inks of different concentrations of hydroxyethyl-cellulose additives and the responses to relative humidity changes will be discussed.

TABLE OF CONTENTS

1. INTRODUCTION

There are many industrial pursuits seeking to exploit the unique chemical and physical properties of coinage metal nanoparticles (NP). Coinage metals include copper, silver, gold, and platinum. Fuel cell catalysis, custom printed electronics, chemotherapeutics, environmental monitoring, and sensor devices include some of the current technological applications incorporating nanoparticle research[29,30]. Functional properties of nanoparticles (mechanical, electromagnetic, biological) are distinct from that of their bulk metal counterparts and are determined by surface chemistry interactions thanks to their high surface area-to-volume ratio. As such, features of nanoparticles including size, shape, and composition all determine nanoparticle functionality[29]. Nanoparticle function is highly dependent on reagent choice and synthesis methods, allowing for customization of nanoparticle properties. Thin film sensor devices can be fabricated which utilize nanoparticles for analyte signal detection and transduction. There are different classifications of sensor devices with medical applications for which the nanoparticles of interest to this study, silver-copper nanoparticles, would be suitable for. Wearable sensor devices, often smart watches, track simple biological metrics like heart rate and blood oxygen saturation. These devices are becoming ubiquitous in the developed world. Fitbit, just one of many companies that specialize in sports fitness devices, sold over 10.6 million units in 2020 alone[1]. The last decade has seen tremendous initiative in expanding the capabilities of wearable sensing devices which could revolutionize healthcare practices. One example would be skin patches capable of electrochemical glucose monitoring. Self-monitoring of blood glucose levels is an integral practice in the management of Diabetes Mellitus, a metabolic disorder that was

the 7th leading cause of death in the United States in 2019[33,34]. Commercially available methods for monitoring blood glucose include traditional finger stick blood testing units and subdermal units that automatically dispense insulin as necessary (**Figure 1.1)**.

Figure 1.1 Images of a wearable glucose sensing device monitoring blood glucose via sweat (Left) and the traditional blood glucose monitoring technique of a finger stick blood test (Right).

Both less invasive and ideally lower cost than traditional glucose monitoring methods currently available, wearable patches that monitor blood glucose levels would do so from the wearer's sweat[22], eliminating the need for blood samples. Another classification of sensors are breath sensors which can detect the presence of volatile organic compounds

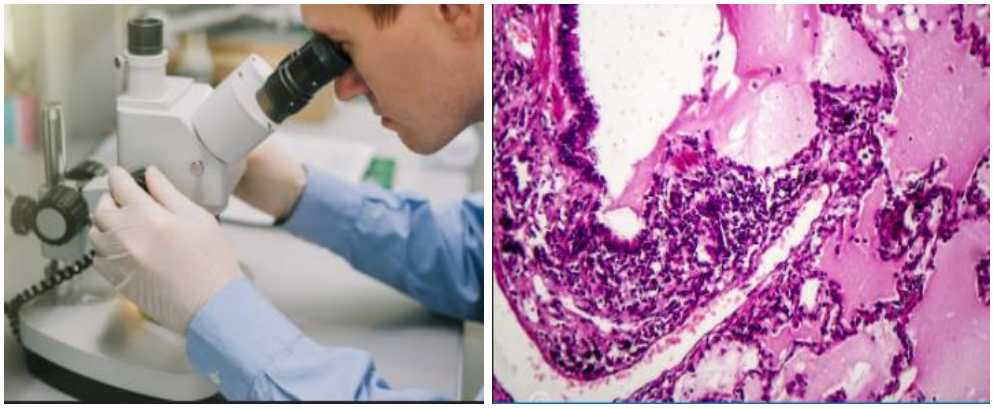

Figure 1.2 Biopsied tissue being examined via light microscope (left). Histological slide of lung adenocarcinoma stained with hematoxylin & eosins.

(VOCs) for the purposes of screening for disease and early intervention care. 2-butanone and 3-hydroxy-2-butanone, for example, are characteristic VOCs exhaled by individuals with lung cancer that are not appreciably present in healthy individual breath samples. An estimated 46% of patients screened for lung cancers via biopsy (**Figure 1.2)** are biopsied again prior to diagnosis[23]. Those biopsied for lung cancer face risk of complications from the procedure like pneumothorax and hemorrhage – risk which could be completely mitigated. Breath sensors would ideally present a reliable, non-invasive alternative for the early detection of lung cancer[24]. Lung cancer is not the only disease state that possesses a unique excretory VOC signature (**Table 1.1**). Styrene, nonanol, and hexadecane may indicate a patient suffers from ovarian cancer[24]. Acetone in the sweat suggests diabetes. Individuals suffering from oral cancer or submucous fibrosis have elevated concentrations of lactate dehydrogenase in their saliva. Even urine samples can be indicative of disease states like cardiovascular disease, diabetic nephropathy, thyroid disease, and more[24]. There is global incentive for the creation of low-cost, non-invasive, and easy to use biosensing devices for the early detection of disease. Very powerful disease detection techniques including immunohistochemical methods like enzyme linked immunosorbent assays (ELISAs) or immunofluorescence assays rely on sensitive, costly instruments and demand a level of expertise making such techniques unavailable or untenable – particularly in the developing world[33]. Accessibility to reliable testing may lead to drastic improvements in lifespan and quality of life globally. Ourworlddata.org defines burden of disease as a concept that is essentially the sum of morbidity and mortality. They report that the years of life lost to premature death worldwide in 2017, which is “the sum of the differences between each person’s age of death and their life

expectancy at that age", disease and disability accounted for the loss of a staggering 853 million years (**Figure 1.3**). 62% of the total burden of disease came from non-communicable disease that year; 9%, of the total came from cancer alone[25]. Early detection can make a world of difference on patient survivorship[26]. Cheap, reliable, and sensitive detection devices for broader use as breath or sweat sensors can be made with silver-copper nanoparticles (AgCu-NPs). AgCu-NPs, used in this study, are at the cutting edge of industry currently. They can be formulated into semi-conductive inks and printed on substrates as thin film sensors to reduce production costs[29]. To the author's knowledge, those developed by the Zhong Group at Binghamton University represent major innovations in synthesis and sintering conditions. These can be synthesized under mild aqueous conditions, retain conductivity comparable to pure silver nanoparticles,

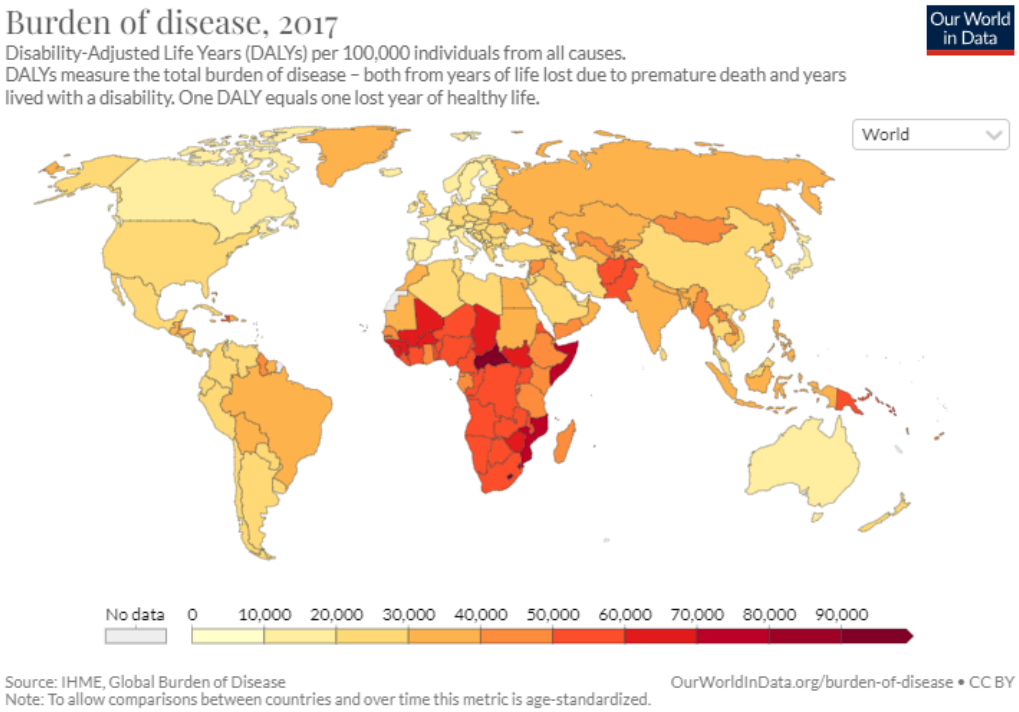

Figure 1.3 Burden of disease heatmap for 2017 (See image for source).

reducing production costs compared with purely silver formulations through copper doping[29,30]. As a nanoalloy, they display a heterogenous distribution of silver and copper atoms rather than typical core-shell structures[17]. Both silver and copper nanoparticles possess distinct localized surface plasmon resonance bands[33]. AgCu-NPs display a lone local surface plasmon resonance (LSPR) peak partway between that of silver and copper that is characteristic of the nanoalloy composition[30]. This optical property is used to verify successful NP synthesis. AgCu-NPs can be mixed with nonconductive molecules into semi-conductive inks or pastes, referred to in this work as nanoinks, and applied as a thin film on a suitable substrate. Thin film sensors made with AgCu-NPs can take advantage of their unique optical, electrical, or magnetic properties for analyte detection. Optical responses come in the form of LSPR red shifting after the adsorption of biomolecules. This is caused by changes in the local refractive index of the thin film[33]. Electrical resistance-based sensors rely on any perturbation to the self-assembled network that spontaneously forms as the thin film dries[2]. Exposure to humidity or VOCs disturbs the self-assembled network and elicits a sensor response[30,35]. This phenomenon is central to the research performed in this study and will be discussed in more detail shortly. Nanoinks can be successfully inkjet, screen, and laser printed onto a variety of substrates. Paper is commonly chosen; it is an environmentally friendly substrate option which is flexible, porous, and cost-effective for production of printed devices and end-of-life disposal[10]. Physical and chemical properties of nanoinks can be modified with the addition of inert or synergistic compounds that properties of the finished product. Cellulose and its derivatives are frequent additions to nanoinks. Cellulose, among alternatives including chitosan, spider silk, or gelatin, is the most abundant naturally

occurring biopolymer in the world[6]. It is a linear polymer composed of beta 1-4 glycosidic bonds (**Figure 1.4**). It is a major structural component of plant cell walls.

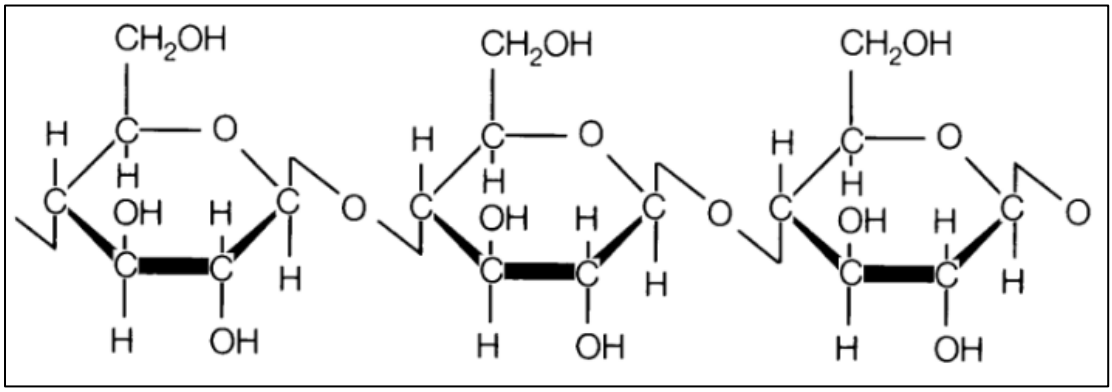

Figure 1.4 Molecular structure of cellulose. Note the beta 1,4 glycosidic bonds.

Cellulose is harvested industrially from tree wood as lignocellulose or a variety of agricultural waste sources including wheat, straw, soy husks, coconut husks, and banana rachis[11]. Cellulose is an excellent insulator and dielectric compound, with a dielectric constant of roughly 6.12[10]. It also acts to increase ink viscosity through gel formation, as well as interesting electrorheological effects under an applied electric field[11]. ink binding affinity for polar VOCs[11]. Nanoink thin films sinter rapidly at ambient temperature[30]. Components of the nanoink spontaneously form complex interconnected matrices in what is referred by the literature as a self-assembled network (SAN). The organization of molecules within the SAN determine the electrical properties of thin films. Percolation theory helps relate electrical properties of thin films and the molecular constituency of their SAN. In basic terms, thin films have conductive and nonconductive components. Electrical conductivity of thin films is directly proportional to the size, shape, and distance between conductive components[2] (**Figure 1.5**). AgCu-NPs are purely conductive and thus unsuitable for electrical resistance-based sensing. Nonconductive additives such

as ethylene glycol, an insulator and thickening agent, are necessary to create semi-conductive thin films appropriate for sensing applications.

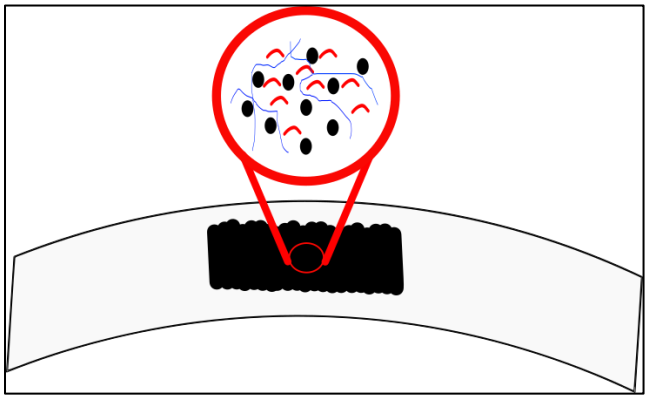

Figure 1.5 Example of nanoink thin film applied on substrate. Black dots represent conductive AgCu-NPs, red (ethylene glycol) and blue (hydroxyethyl cellulose) lines nonconductive molecular spacer molecules which together form spontaneously a self-assembled network on the substrate.

Percolation theory suggests that there exists a concentration range of nonconductive additives which establish a threshold within which optimal electrical resistance exists. Below this threshold, thin films are too conductive; above it, they are too resistant and therefor insensitive[35] (**Figure 1.6**).

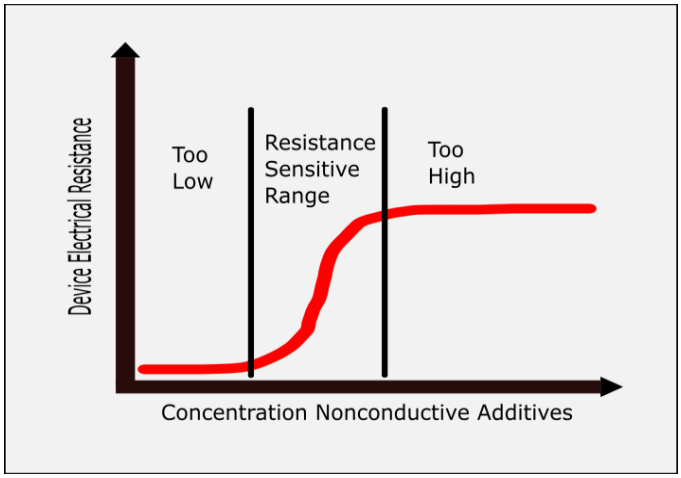

Figure 1.6 Diagram illustrating hypothetical thin film electrical resistance dependence on nonconductive additive concentration in nanoinks. Percolation theory suggests a threshold exists wherein thin films show optimal electrical resistance for use in electrical resistance-sensing.

Problems may arise when using AgCu thin film sensor devices when used as sweat or breath sensors. Exposure to high relative humidity, as in the case of expired breath or sweat, which are saturated with water, can dramatically and in some cases irreversibly reduce the resistance of sintered ink traces of certain silver-copper nanoalloy compositions. Vapor-induced sintering is a well-known phenomenon by which the introduction of water vapor effectively reduces interparticle space through a necking effect[30] (**Figure 1.7**).

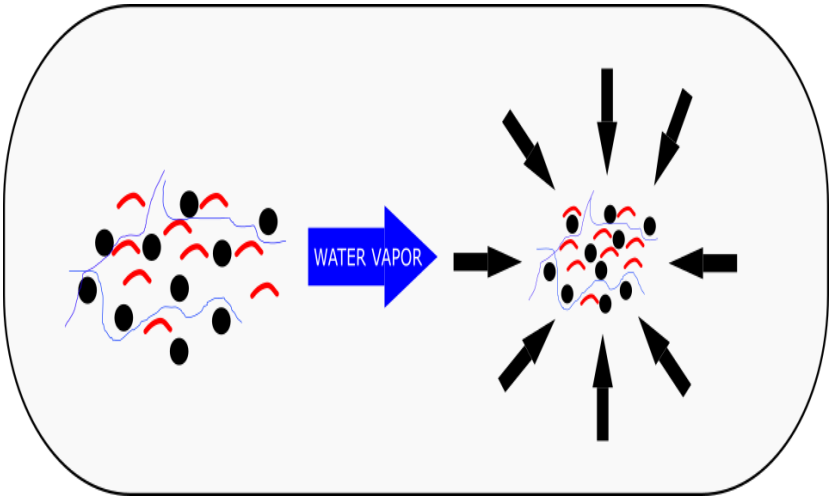

Figure 1.7 Water vapor effectively reduces interparticle distance within SANs of thin films and dilutes nonconductive additive concentrations. AgCu nanoinks of certain compositions undergo further sintering as a result. This may render thin films unusable for sensing.

Water vapor also reportedly diminishes the effective concentration of cellulose or its derivatives in ink formulations using it as an insulator, increasing trace conductivity. This reduction in electrical resistance can render nanoink traces useless for signal detection. Silver-copper nanoalloys synthesized with proportionately more silver are resistant to vapor-induced sintering, while those which are comprised of a greater amount of copper will see a precipitous fall in resistivity[29,30]. Other setbacks of using coinage metal

nanomaterials include cost and toxicity. Currently, suspected modes of metal nanoparticle cytotoxicity include the release of harmful metal ions and the generation of reactive oxygen species[28]. Silver nanoparticles display desirable antimicrobial effects, and has seen incorporation into cosmetics, soaps, textiles, building materials, and much more. One troubling result of this broad-spectrum use of silver nanoparticles is the contamination of water and soil, which has had deleterious effects on aquatic animals and plants, respectively. Silver nanoparticles can even accumulate in tissues of animals raised as livestock to be eaten[28]. More cost-effective, less toxic, and environmentally friendly alternative nanomaterials to coinage metal for the construction of biosensors are also being researched. One particularly exciting alternative to coinage metal nanomaterials are carbon nanotube-cellulose composites, such as the aerogel made by Qi et al. (2014). This composite successfully detected ethanol vapor via changes in electrical resistance. Carbon is an appealing alternative to coinage metals for use in biosensing nanomaterials not only because it is significantly less toxic, but it is able to be captured from the atmosphere[27]. The purpose of this study is to investigate any effects of varying the concentration of nonconductive additives in nanoinks made with AgCu-NPs.

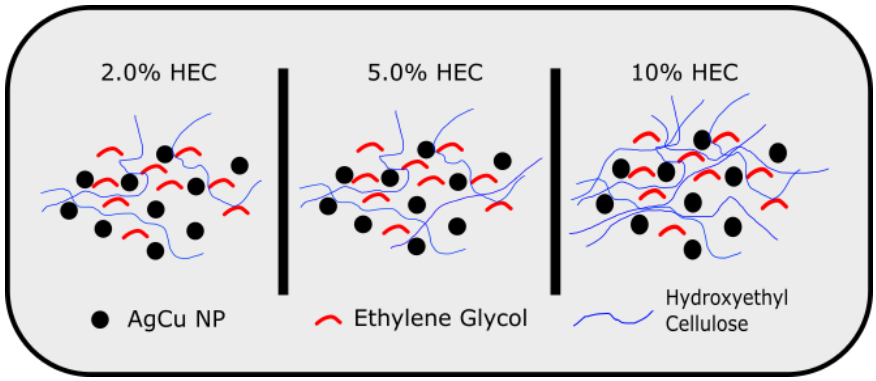

Figure 1.8 Diagram showing the molecular view of SANs formed from nanoinks with varied hydroxyethyl cellulose (HEC) concentration. Percolation theory predicts greater thin film electrical resistance as concentration of the nonconductive additive HEC increases.

Two nonconductive compounds will be added to nanoinks: ethylene glycol, which will remain at a constant concentration in each ink formulated, and hydroxyethyl-cellulose (HEC),a cellulose derivative whose concentration will be varied (**Figure 1.8**). It is hypothesized that a range of HEC concentrations exists with optimal device sensitivity that also display physical resistance to vapor-induced sintering.

2. EXPERIMENTAL METHODS

2.1 Chemicals

In accordance with the research previously conducted in our group by Robinson et al. (2022), chemical precursor reagents already purchased from Millpore-Sigma were available and used in these experiments. The metal reagents used were silver nitrate ($AgNO_3$, ≥ 99.998%) and copper(II) nitrate trihydrate ($Cu(NO_3)_2 \cdot 3H_2O$, ≥ 99%). To prevent particle aggregation, trisodium citrate dihydrate ($Na_3C_6H_5Na_3O_7 \cdot 2H_2O$, ≥99.0%) was added as a capping agent. Sodium borohydride ($NaBH_4$, ≥ 98%) was used as the reduction agent for each synthesis. Hydroxyethyl-cellulose and ethylene glycol were both used in ink formulation.

2.2 **Synthesis**

Silver-copper nanoalloy particles were synthesized according to the procedure established by Robinson et al. 2022. Synthesis parameters were upscaled to 10 times that reported by Robinson for a greater yield of particles with each attempt and to demonstrate the scalability of the procedure. To begin, 400 mL of distilled water (18.2 MΩ) was added to a triple-rinsed 2000 mL round bottom flask. The flask was sealed with a magnetic stir bar and pure nitrogen gas fed from tanks through a Schlenk line to reduce

oxygen saturation and create an inert reaction environment. Reagents were added to the reaction vessel after a half hour passed. First, 1mL of 1M copper(II) nitrate was added to the vessel. Immediately following this was an addition of 1mL 0.88M trisodium citrate dihydrate. A color change from faint blue to brilliant blue was noted in the reaction vessel (**Figure 2.1)**. 1mL of 1M silver nitrate was then added to the flask with no significant change to solution color.

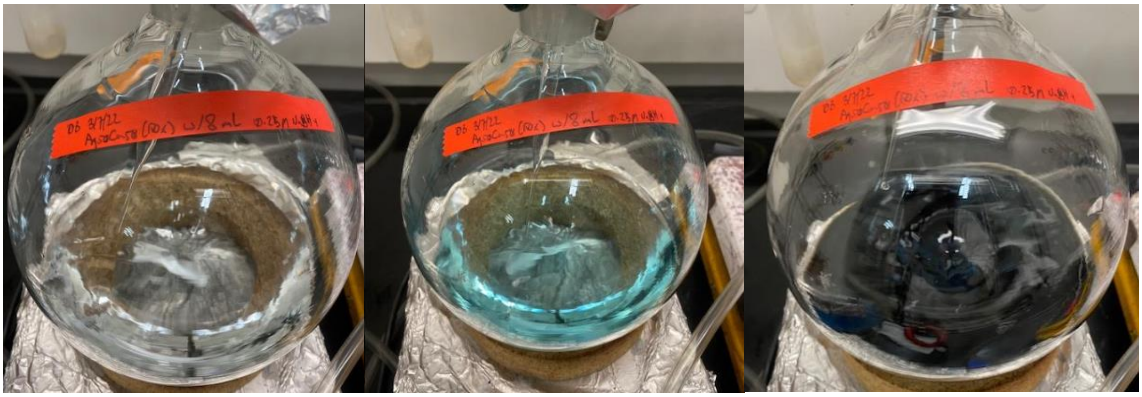

Figure 2.1 Synthesis of Ag55Cu45 nanoparticles. Reaction vessel with 400 mL distilled water sealed under tank fed nitrogen gas (**Right**). Reaction vessel after the addition of 1.0mL 1.0M Copper Nitrate, 1.0mL 0.88M Sodium Citrate, and 1.0mL 1.0M Silver Nitrate (**Middle**). Reaction vessel after slow, dropwise addition of 8.0mL 0.25M Sodium Borohydride **(Left).** Note the dramatic change in color from a brilliant blue to dark caramel after the addition of borohydride, indicating the successful reduction of silver in the solution.

8mL of the reducing agent sodium borohydride (0.25M) was slowly added dropwise to the reaction vessel over a period of 10 minutes. Great care was taken to not exceed additions of 0.8mL per minute. The solution color immediately darkened to a deep cola-caramel after the addition of the first few drops of the reducing agent. The reaction flask remained sealed under tank-fed nitrogen gas supplied through a Schlenk line for one hour following the addition of all precursor reagents. Successful synthesis of silver-copper nanoalloy particles was achieved via UV-Vis confirmation of the expected LSPR [30].

2.3 **Nanoink Formulation**

Five conductive inks were formulated using 30% SCNP by weight. 60% mass of each ink came from hydroxyethyl-cellulose solutions of increasing concentration (2.0%, 3.5%, 5.0%, 7.0%, and 10% by wt). The final 10% mass composition for each ink came from ethylene glycol. Inks were stored at 5 ℃ when not in use.

2.4 **Instrumentation and Measurements**

2.4.1 UV-Vis Spectroscopy

UV-Vis spectroscopy was performed to confirm the successful synthesis of silver-copper nanoalloy particles. The spectrophotometer used was an Agilent 8543 UV-Vis spectrophotometer equipped with a tungsten and deuterium lamp and a range of 200-1100 nm. Disposable cuvettes were used. A cuvette filled with deionized water was used to blank the instrument. Sample cuvettes contained 150µL of the synthesis product and filled to the mark with deionized water.

2.4.2 Inductively Coupled Plasma-Optical Emission Spectroscopy

Inductively Coupled Plasma-Optical Emission Spectroscopy (ICP-OES) was used to determine the elemental composition of the AgCu NPs. The samples were prepared with concentrated nitric acid and left to decompose the solutions for 1 hour. After the decomposition, the remaining nitric acid was boiled off. The metallic components left in solution after burning all the acid were mixed with DI water and left to cool for another 1 hour. Then, 10 mL of the metal-water mixture was pipetted and analyzed with the ICP-OES instrument.

2.4.3 Transmission Electron Microscopy

Transmission Electron Microscopy (TEM) was used to capture images of the NP surfaces for identifications of NP size, shape, and structure. JEOL JEM-ARM200F instrument was used and operated at 200 kV.

2.4.4 Electrical Resistance Measurements

Electrical resistance was measured using a BK Precision 393 multimeter with an IR USB connection for two probe measurements[29]. Humidity and temperature data was collected using a raspberry pi device equipped with a humidity and temperature sensing device which captured data points in one-second intervals during testing.

3. RESULTS & DISCUSSION

3.1. Composition and Morphology of AgCu Nanoparticles

The bimetallic composition of the AgCu NPs is controlled by the feeding ratio of the metal precursors in terms of the moles of $AgNO_3$ and $Cu(NO_3)_2$ in the solution. The NP compositions were determined by ICP-OES. The molar feed percentages of Ag and Cu in the solution were compared to the Ag and Cu composition in the NPs that was determined by ICP. As shown by the plot of Ag% in the NPs vs. Ag% in the solution in Figure 1, indicative of a 1-to-1 relationship.

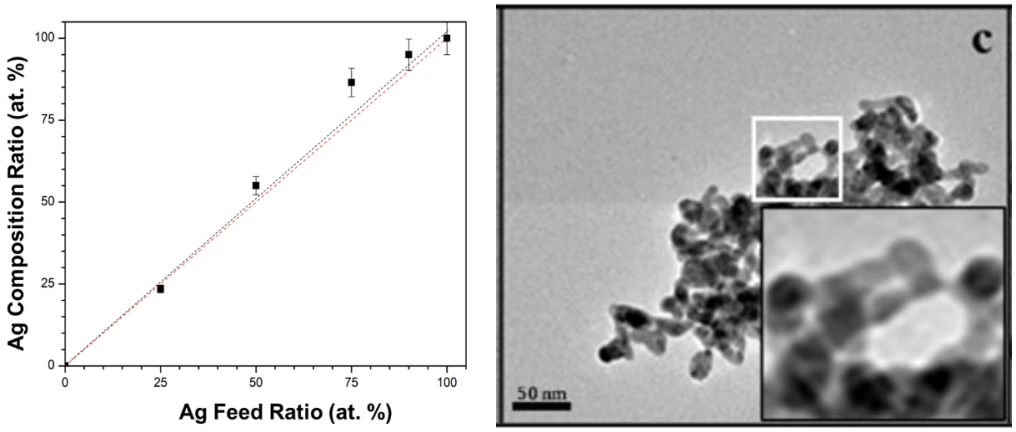

Figure 3.1: Left: Relationship between the molar feed ratio of Ag and ICP-OES determined Ag composition in AgCu NPs (The red dashed line represents an ideal 1:1 relationship) **: Right:** TEM images of $Ag_{55}Cu_{45}$ NPs (Scale Bar: 50 nm) with an inset showing a magnified area[35]

Figure 3.1 (**right**) shows a representative TEM image for the as-synthesized AgCu NPs. AgCu nanoparticles showed the presence of similar-sized NPs and a clear increase in particle size due to the aggregation of the neighboring particles. The tendency of aggregation is clearly increased as the Cu% is increased in the NPs, as shown for $Ag_{55}Cu_{45}$ NPs. The NPs have an average radius of 9.91 ± 2.53 nm. The NPs show a network feature due to a high degree of aggregation. It is evident that the bimetallic NPs exhibit a greater tendency of aggregation under room temperature on the surface of carbon film of the TEM grid. The increases in particle size for the bimetallic NPs reflect a surface-mediated Ostwald Ripening process, where the larger AgCu nanoparticles were formed at the expense of smaller particles on the surface of carbon film substrate.

3.2. UV-Vis Characterization of AgCu Nanoparticles

To demonstrate the scalability of the wet chemical methods previously used for AgCu nanoparticles (NPs) previously explored by this group, syntheses were performed at 10x scale compared to that already reported. For example, if 100µL of 1M copper nitrate would be added in to a 1x synthesis reaction vessel, 1.00mL of the same would be added to the 10x synthesis reaction vessel. Since AgCu NPs possess distinct LSPR maxima, success of the synthesis was confirmed via UV-Vis spectroscopy to determine the synthesized product's spectral profile. LSPR is a phenomenon produced by the absorption of incident light of wavelengths capable of inducing oscillations in conduction electrons within the synthesized particles. Spectral profiles for AgCu NPs with different metal reagent precursors made at 1x were available thanks to previous research efforts (**Figure 3.2**). A maximum absorbance wavelength of 396 nm was observed in the 10x $Ag_{55}Cu_{45}$ sample, which matches very closely to 1x $Ag_{55}Cu_{45}$ sample maximum absorbance wavelength of 395 nm. It is interesting to note that more incident light was absorbed by the 10x sample compared to the 1x sample. Although more NPs are

theoretically being produced in upscaled synthesis, the same concentration of particles should be contained in 150µL samples of each scale. Beer's Law connects absorbance and analyte concentration: **A = εbC,** where A is absorbance (a.u.), **ε** is the molar extinction coefficient [L / (mol*cm)], b is the pathlength (cm), and C is molar concentration (mol/L). Given the linear relationship between absorbance and concentration, it appears that a greater concentration of particles was found in the upscale synthesis, however the reasons behind this difference were not explored in this study. One likely explanation to account for this apparent concentration difference is that a nanoparticle concentration gradient was established within the reaction vessel after magnetic stirring ceased between the time synthesis was complete and when a sample was collected for spectroscopic analysis. The LSPR would remain distinct for nanoparticles of this precursor feed ratio regardless of sample concentration.

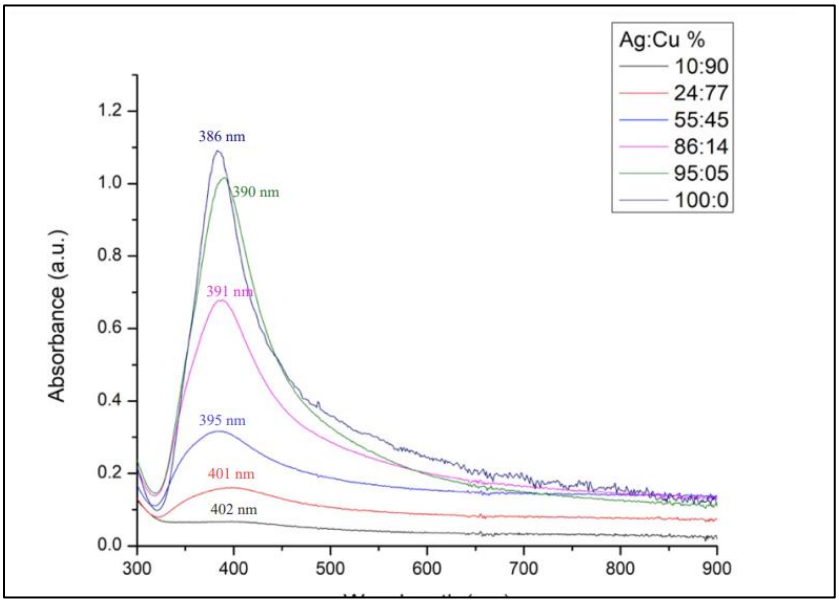

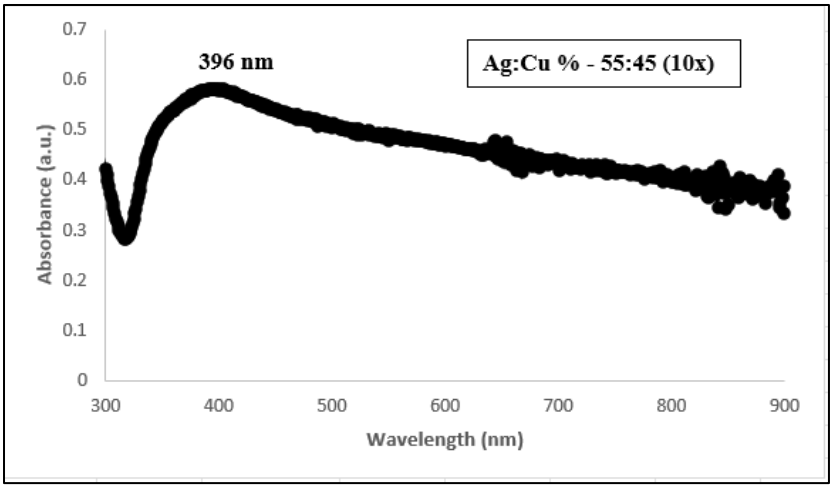

Figure 3.2 UV-Vis spectra of AgCu nanoparticles synthesized with different reagent feed ratios result in different absorbance (**top**[30]). UV-Vis spectrum of 10x synthesis showing a maximum absorbance wavelength of 396 nm, which closely agrees with the 1x synthesis maximum absorbance wavelength of 395 nm.

3.3. Electrical Properties of the Nanoinks under Nitrogen and Controlled Relative Humidity

The goal of this study was to explore changes in the response behavior of silver-copper nanoinks with varied hydroxyethyl-cellulose concentrations when exposed to humidity. Five AgCu nanoinks with varied concentrations of hydroxyethyl-cellulose were formulated for the purposes of this study (**Table 3.1)**. Hydroxyethyl-cellulose (HEC) solutions were added at a constant weight percentage to the final nanoink formulation, however, the amount of HEC contained in each HEC solution varied by weight. Nanoinks were homogenized by ultrasonication for 15 minutes. Immediately afterwards, traces were applied with a clean Pasteur pipette tip to printed IME electrode devices, brushed until evenly applied across the electrodes, then allowed to sinter under ambient conditions overnight (**Figure 3.3**). IME devices with sintered ink traces were placed in a sealed container with multimeter electrodes attached to complete the circuit, allowing for the control of atmospheric conditions.

Table 3.1: Nanoink Composition

AgCu Nanoink Formulations	
AgCu NPs	30% wt
HEC	60% wt*
Ethylene Glycol	10% wt
***2.0%, 3.5%, 5.0%, 7.0%, 10% HEC wt solns**	

Once sealed, chambers containing the IME sensor devices were purged with tank-fed nitrogen gas with a pressure of 20psi for 10 minutes. Tank-fed nitrogen gas at the same pressure also served as a carrier gas to deliver water vapor to the sealed chamber during testing. A Cole Parmer SCFH Air flow control was used to control the level of humidity reached in the testing chamber (**Figure 3.3**).

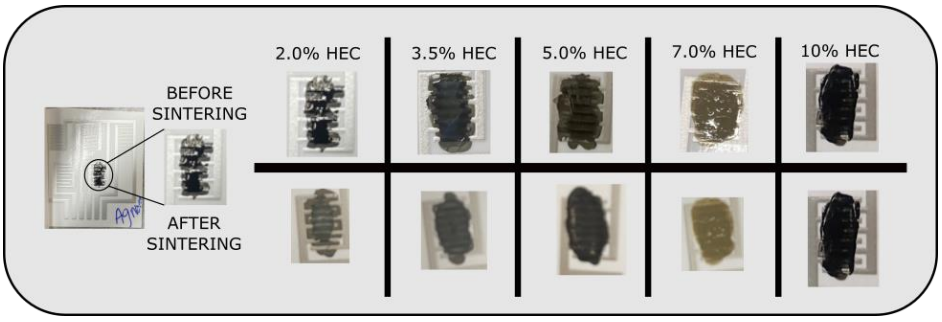

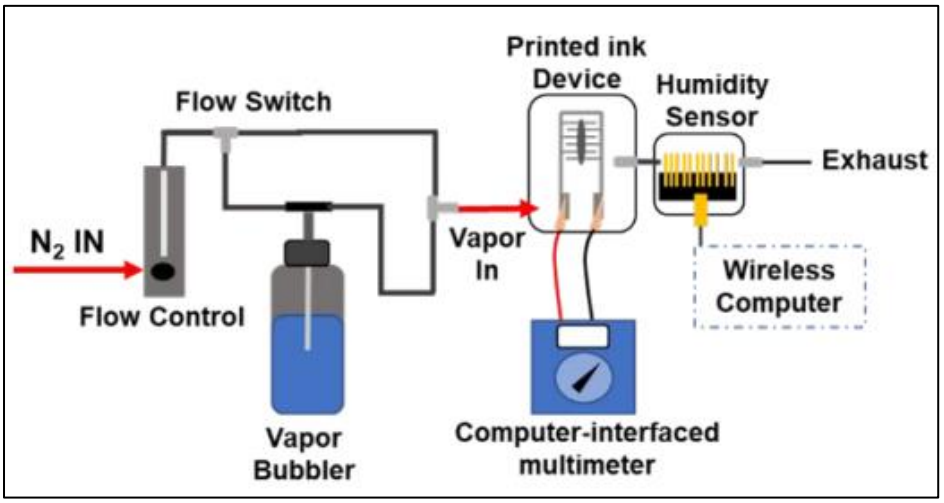

Figure 3.3 Example images of nanoink applied with a Pasteur pipette tip then brushed evenly to a printed IME device electrode which was allowed to sinter under ambient conditions overnight (**Top**). Schematic of experimental setup (**Bottom**[29]).

Devices were tested in 30-minute cycles. Three flow controller settings (0.1, 0.2, or 0.4) were chosen to vary the final relative humidity level achieved within the testing chamber during each 30-minute cycle. Water vapor was allowed to enter the chamber for 20 minutes, followed by a 10-minute nitrogen gas purge.

Figures 3.4-3.6 depict sensor response to chamber humidity in the form of changes in resistance. In general, a greater initial resistance was observed in devices with sintered nanoink traces of increasing HEC concentrations. Initial resistance measuring 60MΩ or greater overloaded the multimeter used in this study; therefore, the maximum resistance values reported were arbitrarily set to 60 MΩ. The lowest initial resistance values were observed from the 2.0% (~180Ω) and 3.5% (~4.4MΩ) HEC nanoinks. Both the 2.0% and 3.5% inks experienced water vapor-induced sintering during testing after testing as evidenced by a permanent decrease in device resistance. The 5.0%, 7.0%, and 10% HEC nanoinks all had initial resistance measuring greater than or equal to 60MΩ. An increasing trend in initial nanoink electrical resistance can be attributed to the increasing hydroxyethyl cellulose concentration within the ink, which acts as a dielectric insulator and increases interparticle distance[29]. HEC molecules are capable of forming molecular matraces comprised of inter-and-intramolecular bonds, including hydrogen bonds and weak non-polar bonding[13]. Increasing the concentration of hydroxyethyl cellulose in the final ink formulation increases steric bulk and ink viscosity such that the capacity for water molecules or nanoparticles to migrate is reduced[31]. Processes like surface-mediated Ostwald ripening would be directly inhibited as they proceed via the spontaneous

dissolution of small nanoparticles to form larger ones, reducing the surface-to-volume ratio and lowering free surface energy. Although the hydrophillic hydroxyl side chains of HEC strongly attract water molecules because of their ability to participate in hydrogen bonding, the equilibrium water adsorption remains low with increasing concentration of HEC under high relative humidity[31]. Inks with a greater concentration of hydroxyethyl cellulose may also exhibit greater tolerance to water vapor exposure because of nanoparticle stability. The surface free energy of nanoparticles decreases with increasing HEC concentration.

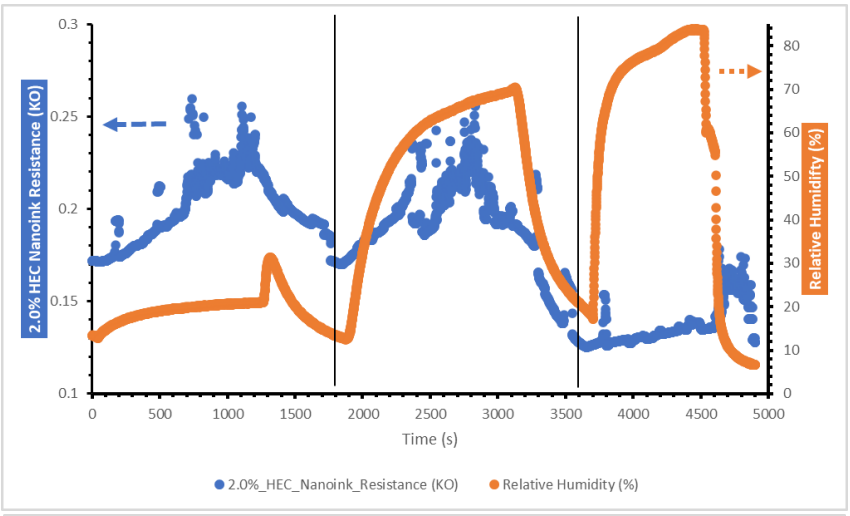

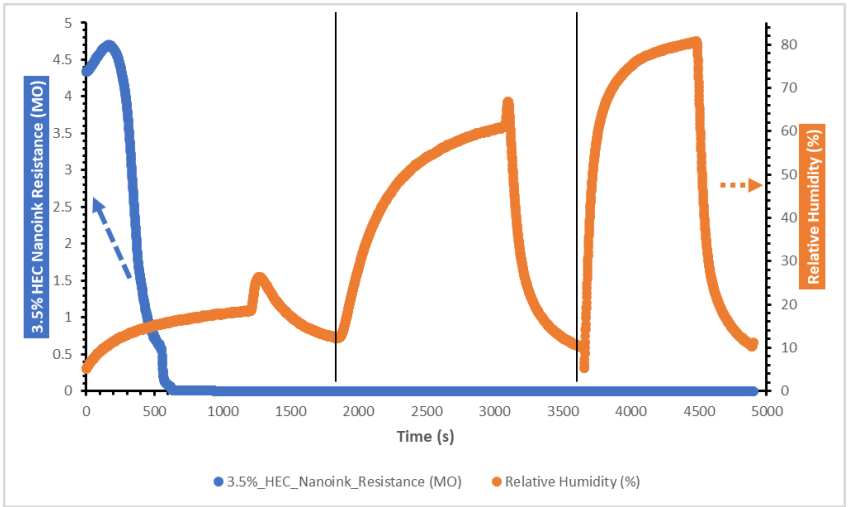

Figure 3.4 2.0% HEC nanoink sensor resistance response to changing relative humidity over time (**Top**). 3.5% HEC nanoink sensor resistance response to changing relative humidity over time (**Bottom**). Vertical dashed lines divide 30-minute test cycles. Test cycles consisted of 20 minutes water vapor exposure and 10 minutes nitrogen purge. Sensor response to increased water vapor exposure is shown left-to-right over time. Note the final resistance value for both nanoinks shown was lower than the initial, indicating vapor-induced sintering occurred.

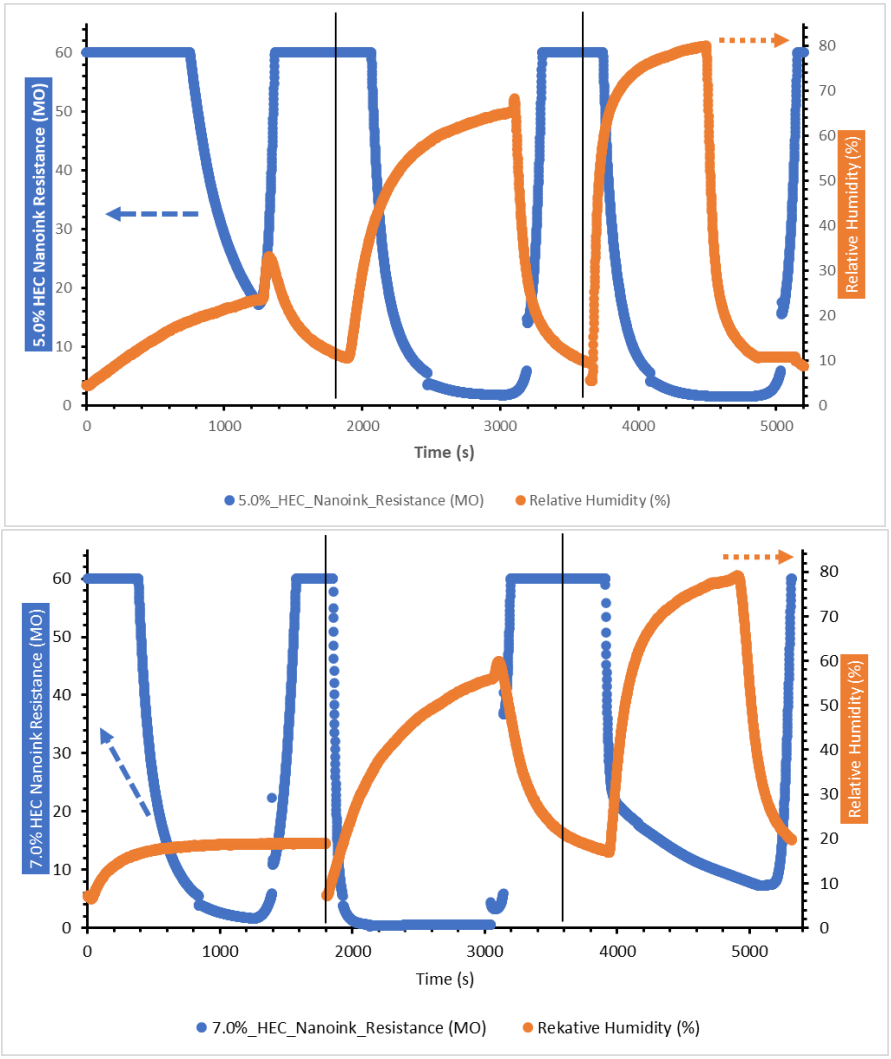

Figure 3.5 5.0% HEC nanoink sensor resistance response to changing relative humidity over time (**Top**). 7.0% HEC nanoink sensor resistance response to changing relative humidity over time (**Bottom**). Vertical dashed lines divide 30-minute test cycles. Test cycles consisted of 20 minutes water vapor exposure and 10 minutes nitrogen purge. Sensor response to increased water vapor exposure is shown left-to-right over time.

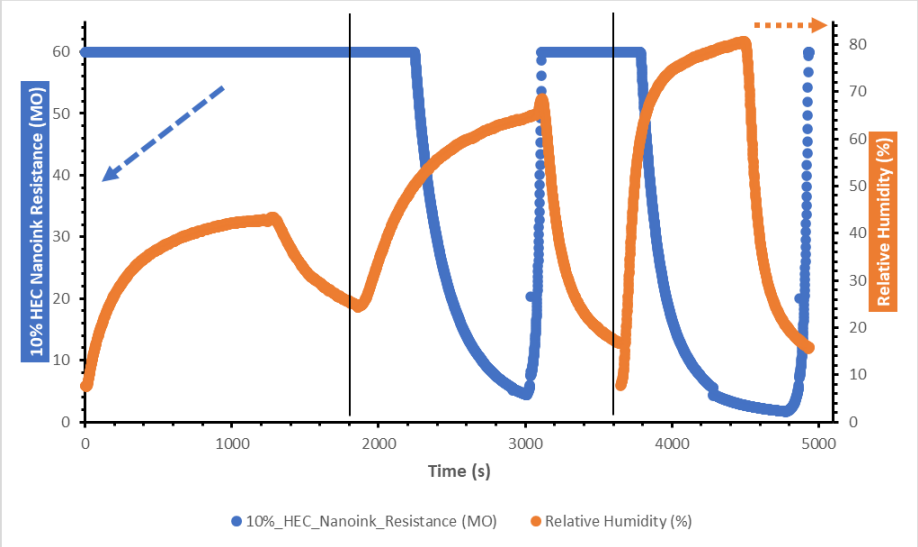

Figure 3.6 10% HEC nanoink sensor resistance response to changing relative humidity over time. Vertical dashed lines divide 30-minute test cycles. Test cycles consisted of 20 minutes water vapor exposure and 10 minutes nitrogen purge. Sensor response to increased water vapor exposure shown left-to-right over time. Note this nanoink did not respond to changing relative humidity until the second test cycle.

Hydroxyl groups and carboxyl groups found on HEC possess lone pairs able to coordinate with Inks with higher HEC concentration demonstrated enhanced resistance to vapor-induced sintering as initial resistance values (>=60MΩ) were restored when wator vapor was purged from the testing chamber. Resistance measurements for these three inks dropped in linear or near-linear proportion to the relative humidity within the testing chamber. **Figure 3.7** plots device resistance (MΩ) as a function of relative humidity (%) for the testing cycles where sensors were exposed to the greatest concentration of water vapor. Interestingly, resistance values for the 2.0% HEC nanoink peaked when relative humidity was greatest.

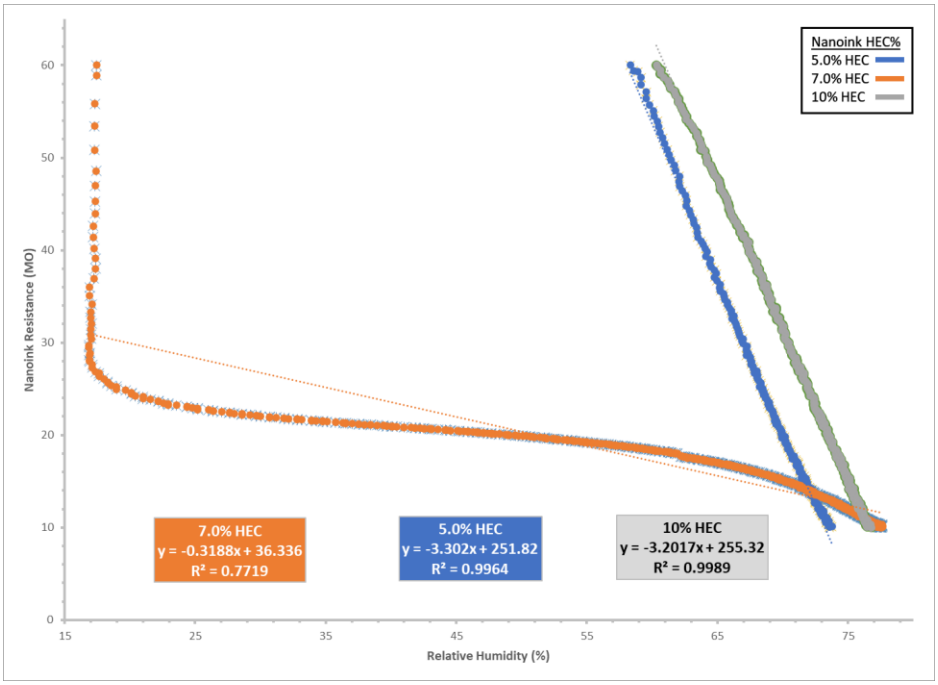

Figure 3.7 Nanoink resistance plotted as a function of test chamber relative humidity. Data for the 5.0%, 7.0%, and 10% HEC nanoink sensors from the final test cycle (exposure to the greatest concentration of water vapor) is shown. Note the strongly linear dependence of resistance on relative humidity for the 5.0% and 10% inks. Linearity breaks down below 10MΩ; above 60MΩ is unknown. The logarithmic response nature of the 7.0% HEC nanoink may reflect defects in ink preparation.

This study sought to characterize any differences in nanoink trace response to humidity when hydroxyethyl cellulose concentration is varied in nanoink formulation. The goal this research contributes to is the eventual production of a cost effective, easy-to-use biosensor. Silver-copper nanoparticles possess distinct physical and chemical properties which make them ideal for biosensor applications, functioning as signal transducers in sensor devices. Such devices could be used for the screening and early detection of diseases including several types of cancer and metabolic disorders like Diabetes Mellitus. Since biological samples to be screened for signs of disease such as sweat or respiration would be saturated with water, water and water vapor-induced sintering remains a major challenge to the durability and reusability of such a sensor

device. Changes in nanoink additive concentration (T**able 3.2)** can directly impact the sensor initial resistance and therefore sensitivity (**Figure 3.8**).

Table 3.2 Nanoink Mass composition (Dry)

Nanoink Mass Composition (Dry)					
HEC Stock (wt%)	**2.0%**	**3.5%**	**5.0%**	**7.0%**	**10%**
AgCu NP (g)	0.066	0.1599	0.1329	0.1386	0.0516
HEC (g)	0.004	0.019	0.022	0.032	0.017
Ethylene Glycol (g)	0.022	0.0533	0.0443	0.0462	0.0172
Total Nanoink Mass (g)	0.22	0.533	0.443	0.462	0.172
AgCu NP (wt%)	30%	30%	30%	30%	30%
HEC (wt%)	2%	3.5%	5%	7%	10%
Ethylene Glycol (wt%)	10%	10%	10%	10%	10%

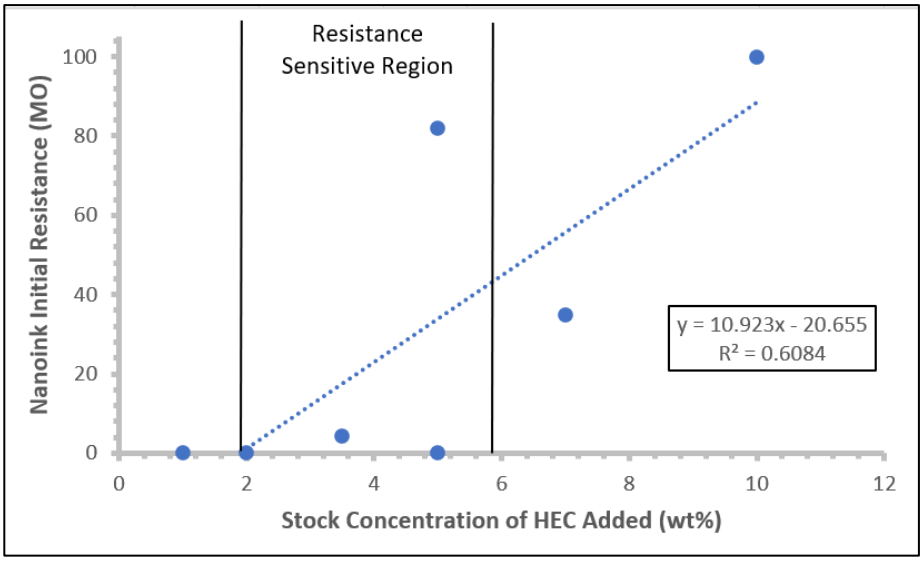

Figure 3.8 Plot of nanoink initial resistance when dry, measured under tank-fed nitrogen for ten minutes vs the stock concentration of HEC (wt%) added to each ink. Recall **Figure 1.6**.

This research helps establish the feasibility of a concentration range wherein nanoink resistance can be tuned for optimal sensitivity with enhanced physical resistance

to further sintering in the presence of water. Based on the findings of this study, nanoink stability against vapor-induced sintering can be increased with increasing the amount of hydroxyethyl cellulose (and likely other cellulose derivatives) in the final ink formulation.

Figure 3.9 shows a diagram representing the differences in nanoink composition on a molecular scale. From left to right, the concentration of HEC added to the nanoink is shown to increase. HEC acts as a dielectric insulator to the nanoink, preventing particle aggregation and increasing the interparticle distance. The electrical conductivity of the HEC-AgNP ink can be described by the percolation theory in terms of the interparticle spatial properties[36] where the conductive composite network consists of the conductive (AgCu NPs) and insulative (HEC, and EG capping/linking molecules as well) components. As the insulative component fraction is gradually increased, the composite network would undergo a conductor-to-insulator transition. Based on the preliminary experimental results for the nanoink at the given EG and NP concentrations, this transition falls likely in the range of 1 – 5%HEC. Nanoinks (30% wt AgCu NPs/60% wt HEC soln./10% wt Ethylene Glycol) with HEC solution concentrations greater than or equal to 5.0% resisted vapor-induced sintering. These inks also displayed a high magnitude of the initial resistance, rendering them out of the range of the multimeter used for the detection. Nanoinks with HEC concentrations of 3.5% or lesser sintered, showing a very small electrical resistance which is basically very conductive and thus not sensitive to the adsorption of the analytes

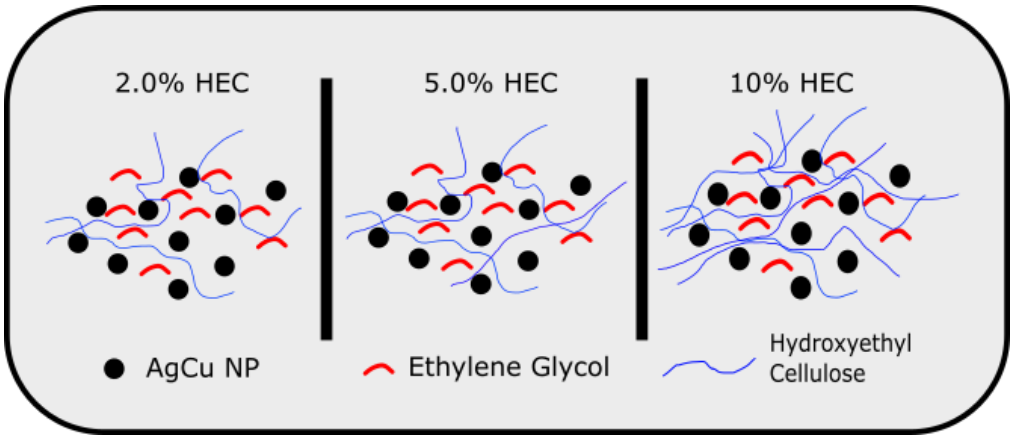

Figure 3.9 Diagram depicting the role of hydroxyethyl cellulose in nanoink traces. As HEC concentration increases, the nanoink becomes more viscous and processes such as Ostwald ripening or vapor-induced sintering are increasingly inhibited, which lead to decreased electrical conductivity of the sintered nanoink.

The optimal concentration of HEC in ink formulation, showing some measurable responses to the adsorption of the analytes, seemed to fall in between 3.5% to 5.0% wt. This is a very rough range identified in this preliminary work for assessing the semi-conductive range of the HEC-AgNP nanoink for sensor fabrication. More accurate identification is needed by performing more experimental measurements with smaller increments of the HEC concentration in the nanoinks in a systematical way in terms of the various components' concentrations (e.g., EG, NPs, etc.).

4. SUMMARY AND FUTURE WORK

The purpose of this study was to investigate and characterize changes in sensor behavior of bimetallic silver-copper nanoinks with varied hydroxyethyl cellulose concentrations. The goal this research contributes to is the fabrication of a sensitive, tunable, cheap biosensor device. Silver-copper nanoparticles, capable of being synthesized using mild wet chemical methods, possess distinct physical and chemical properties which render them useful in biosensor devices used to screen for disease.

Conductive inks formulated with these nanoparticles contain other additives that alter the physical and chemical properties of the final nanoink produced. AgCu NPs undergo vapor-induced sintering, observable through a dramatic, permanent negative change in sensor electrical resistance, when exposed to elevated relative humidity. To prevent an irrecoverable change in resistance and preserve the viability of the sensor device for multiple test cycles, increasing the concentration of hydroxyethyl cellulose has shown to prevent vapor-induced sintering. Too great a concentration of HEC reduces the efficacy of the sensor because initial electrical resistance is too high. Too small a concentration of HEC will fail to stabilize AgCu nanoparticles through reduction of the surface free energy. It is likely that an optimal concentration of hydroxyethyl cellulose lies between 2.0% and 5.0% wt. This concentration range forms the bounds of a resistance sensitive range in which nanoinks remain sensitive to analytes yet physically resistant to vapor induced sintering. Areas for future exploration include further investigation into the resistance sensitive concentration range of HEC in nanoinks, the addition of multiple cellulose derivatives such as carboxymethyl cellulose or nanofiber cellulose crystals nanoink to control ink responsiveness to analytes of a certain polarity. Some of the biological markers for cancers (see above) included nonanol or butanone. Sensor response to these VOCs, mixtures of VOCs, and mixtures of VOCs with water vapor should also be investigated. An additional challenge facing AgCu thin film sensors is selectivity for specific analytes. It was mentioned above that many diseases possess distinct VOC signatures from which preliminary diagnosis might be made. A given breath sample, however, may contain hundreds of VOCs. For effective diagnosis to be made, data from healthy individuals and those confirmed to have the disease could be

collected to establish standards. Principle component analysis is a powerful statistical analysis tool which can be used to compare sensor responses of screened individuals for preliminary diagnosis to be made. Arraying sensors may also increase sensitivity and selectivity of these devices.

5. REFERENCES

1. *Fitbit device unit sales worldwide 2010-2020*. Statista. https://www.statista.com/statistics/472591/fitbit-devices-sold/ (accessed 2022-04-06).
2. Cheng, H.-W.; Yan, S.; Shang, G.; Wang, S.; Zhong, C.-J. Strain Sensors Fabricated by Surface Assembly of Nanoparticles. *Biosensors and Bioelectronics* **2021**, *186*, 113268. https://doi.org/10.1016/j.bios.2021.113268.

3. Peng, P.; Li, L.; Guo, W.; Hui, Z.; Fu, J.; Jin, C.; Liu, Y.; Zhu, Y. Room-Temperature Joining of Silver Nanoparticles Using Potassium Chloride Solution for Flexible Electrode Application. *J. Phys. Chem. C* **2018**, *122* (5), 2704–2711. https://doi.org/10.1021/acs.jpcc.7b10601.

4. Dai, X.; Xu, W.; Zhang, T.; Shi, H.; Wang, T. Room Temperature Sintering of Cu-Ag Core-Shell Nanoparticles Conductive Inks for Printed Electronics. *Chemical Engineering Journal* **2019**, *364*, 310–319. https://doi.org/10.1016/j.cej.2019.01.186.

5. Tsuchiya, K.; Mori, Y.; Kawaguchi, M. Effects of Hydroxyethyl Cellulose and Colloidal Silica Abrasive on the Hydrophilicity of Polished Si Wafer Surfaces. *ECS J. Solid State Sci. Technol.* **2017**, *6* (7), P361. https://doi.org/10.1149/2.0021707jss.

6. Selyanchyn, O.; Selyanchyn, R.; Lyth, S. M. A Review of Proton Conductivity in Cellulosic Materials. *Front. Energy Res.* **2020**, *8*, 596164. https://doi.org/10.3389/fenrg.2020.596164.

7. Qi, H.; Liu, J.; Pionteck, J.; Pötschke, P.; Mäder, E. Carbon Nanotube–Cellulose Composite Aerogels for Vapour Sensing. *Sensors and Actuators B: Chemical* **2015**, *213*, 20–26. https://doi.org/10.1016/j.snb.2015.02.067.

8. Nie, S.; Hao, N.; Zhang, K.; Xing, C.; Wang, S. Cellulose Nanofibrils-Based Thermally Conductive Composites for Flexible Electronics: A Mini Review. *Cellulose* **2020**, *27* (8), 4173–4187. https://doi.org/10.1007/s10570-020-03103-y.

9. Wang, X.; Wu, P. Fluorinated Carbon Nanotube/Nanofibrillated Cellulose Composite Film with Enhanced Toughness, Superior Thermal Conductivity, and Electrical Insulation. *ACS Appl. Mater. Interfaces* **2018**, *10* (40), 34311–34321. https://doi.org/10.1021/acsami.8b12565.

10. Agate, S.; Joyce, M.; Lucia, L.; Pal, L. Cellulose and Nanocellulose-Based Flexible-Hybrid Printed Electronics and Conductive Composites – A Review. *Carbohydrate Polymers* **2018**, *198*, 249–260. https://doi.org/10.1016/j.carbpol.2018.06.045.

11. Choi, K.; Gao, C. Y.; Nam, J. D.; Choi, H. J. Cellulose-Based Smart Fluids under Applied Electric Fields. *Materials* **2017**, *10* (9), 1060. https://doi.org/10.3390/ma10091060.

12. Nasatto, P.; Pignon, F.; Silveira, J.; Duarte, M.; Noseda, M.; Rinaudo, M. Methylcellulose, a Cellulose Derivative with Original Physical Properties and Extended Applications. *Polymers* **2015**, *7* (5), 777–803. https://doi.org/10.3390/polym7050777.

13. Zhao, D.; Zhu, Y.; Cheng, W.; Chen, W.; Wu, Y.; Yu, H. Cellulose-Based Flexible Functional Materials for Emerging Intelligent Electronics. *Adv. Mater.* **2021**, *33* (28), 2000619. https://doi.org/10.1002/adma.202000619.

14. Bourassa, J.; Ramm, A.; Feng, J. Q.; Renn, M. J. Water Vapor-Assisted Sintering of Silver Nanoparticle Inks for Printed Electronics. *SN Appl. Sci.* **2019**, *1* (6), 517. https://doi.org/10.1007/s42452-019-0542-0.

15. Wang, F.; Richards, V. N.; Shields, S. P.; Buhro, W. E. Kinetics and Mechanisms of Aggregative Nanocrystal Growth. *Chem. Mater.* **2014**, *26* (1), 5–21. https://doi.org/10.1021/cm402139r.

16. Zhang, J.; Huang, F.; Lin, Z. Progress of Nanocrystalline Growth Kinetics Based on Oriented Attachment. *Nanoscale* **2010**, *2* (1), 18–34. https://doi.org/10.1039/B9NR00047J.

17. Yan, S.; Shan, S.; Wen, J.; Li, J.; Kang, N.; Wu, Z.; Lombardi, J.; Cheng, H.; Wang, J.; Luo, J.; He, N.; Mott, D.; Wang, L.; Ge, Q.; Hsiao, B. S.; Poliks, M.; Zhong, C. Surface-Mediated Interconnections of Nanoparticles in Cellulosic Fibrous Materials toward 3D Sensors. *Adv. Mater.* **2020**, *32* (36), 2002171. https://doi.org/10.1002/adma.202002171.

18. Kim, J.; Campbell, A. S.; Wang, J. Wearable Non-Invasive Epidermal Glucose Sensors: A Review. *Talanta* **2018**, *177*, 163–170. https://doi.org/10.1016/j.talanta.2017.08.077.

19. Zafar, H.; Channa, A.; Jeoti, V.; Stojanović, G. M. Comprehensive Review on Wearable Sweat-Glucose Sensors for Continuous Glucose Monitoring. *Sensors* **2022**, *22* (2), 638. https://doi.org/10.3390/s22020638.

20. Fu, X.-A.; Li, M.; Knipp, R. J.; Nantz, M. H.; Bousamra, M. Noninvasive Detection of Lung Cancer Using Exhaled Breath. *Cancer Med* **2014**, *3* (1), 174–181. https://doi.org/10.1002/cam4.162.

21. Koroleva, M. Yu.; Yurtov, E. V. Ostwald Ripening in Macro- and Nanoemulsions. *Russ. Chem. Rev.* **2021**, *90* (3), 293–323. https://doi.org/10.1070/RCR4962.

22. Kang, N.; Lin, F.; Zhao, W.; Lombardi, J. P.; Almihdhar, M.; Liu, K.; Yan, S.; Kim, J.; Luo, J.; Hsiao, B. S.; Poliks, M.; Zhong, C.-J. Nanoparticle–Nanofibrous Membranes as Scaffolds for Flexible Sweat Sensors. *ACS Sens.* **2016**, *1* (8), 1060–1069. https://doi.org/10.1021/acssensors.6b00414.

23. Zhang, Y.; Shi, L.; Simoff, M. J.; J Wagner, O.; Lavin, J. Biopsy Frequency and Complications among Lung Cancer Patients in the United States. *Lung Cancer Management* **2020**, *9* (4), LMT40. https://doi.org/10.2217/lmt-2020-0022.

24. Broza, Y. Y.; Zhou, X.; Yuan, M.; Qu, D.; Zheng, Y.; Vishinkin, R.; Khatib, M.; Wu, W.; Haick, H. Disease Detection with Molecular Biomarkers: From Chemistry of Body Fluids to Nature-Inspired Chemical Sensors. *Chem. Rev.* **2019**, *119* (22), 11761–11817. https://doi.org/10.1021/acs.chemrev.9b00437.

25. Roser, M.; Ritchie, H. Burden of Disease. *Our World in Data* **2021**.

26. Miller, K. D.; Nogueira, L.; Mariotto, A. B.; Rowland, J. H.; Yabroff, K. R.; Alfano, C. M.; Jemal, A.; Kramer, J. L.; Siegel, R. L. Cancer Treatment and Survivorship Statistics, 2019. *CA A Cancer J Clin* **2019**, *69* (5), 363–385. https://doi.org/10.3322/caac.21565.

27. Pieri, T.; Angelis-Dimakis, A. Model Development for Carbon Capture Cost Estimation. *Clean Technol.* **2021**, *3* (4), 787–803. https://doi.org/10.3390/cleantechnol3040046.

28. Pulit-Prociak, J.; Banach, M. Silver Nanoparticles – a Material of the Future…? *Open Chemistry* **2016**, *14* (1), 76–91. https://doi.org/10.1515/chem-2016-0005.

29. Robsinton, R. PhD Dissertation. **2022**.

30. Kraus, V. Honors Thesis. **2021**.

31. Henriksson, M.; Berglund, L. A. Structure and Properties of Cellulose Nanocomposite Films Containing Melamine Formaldehyde. *J. Appl. Polym. Sci.* **2007**, *106* (4), 2817–2824. https://doi.org/10.1002/app.26946.

32. Craciun, A. M.; Focsan, M.; Magyari, K.; Vulpoi, A.; Pap, Z. Surface Plasmon Resonance or Biocompatibility—Key Properties for Determining the Applicability of Noble Metal Nanoparticles. *Materials* **2017**, *10* (7), 836. https://doi.org/10.3390/ma10070836.

33. Chamberlain, J. J.; Rhinehart, A. S.; Shaefer, C. F.; Neuman, A. Diagnosis and Management of Diabetes: Synopsis of the 2016 American Diabetes Association Standards of Medical Care in Diabetes. *Ann Intern Med* **2016**, *164* (8), 542. https://doi.org/10.7326/M15-3016.

34. *NVSS - Leading Causes of Death*. https://www.cdc.gov/nchs/nvss/leading-causes-of-death.htm (accessed 2022-05-09).

35. (**Reference**: Richard Robinson, Virginia Krause, Shan Wang, Shan Yan, Guojun Shang, Justine Gordon, Serena Tycko, Chuan-Jian Zhong, Langmuir 2022, ASAP).

36. H.W. Cheng, S. Yan, G. Shang, S. Wang, C.J. Zhongb, Strain Sensors Fabricated by Surface Assembly of Nanoparticles, Biosensors & Bioelectronics, 2021, 186, 113268.

6. ACKNOWLEDGEMENTS

I would like to extend my thanks to everyone who invested time and patience in helping me complete this study. Dr. Chuan-Jian Zhong and Dr. Richard Robinson opened the door for research to me – to them I am most grateful. The Zhong research group has been nothing short of accommodating. Many thanks to graduate students and undergraduate students alike! I am also grateful to Dr. Hirschi and Dr. Guo for their time in sitting on my committee. Many have helped me along the way. In closing, I should like to acknowledge my gratitude of Binghamton University, the Department of Chemistry, and the National Science Foundation and XCEED for providing the means to conduct research for this project